

# Constraints on the decay of dark matter to dark energy from weak lensing bispectrum tomography

Björn Malte Schäfer<sup>1,2\*</sup>, Gabriela Caldera-Cabral<sup>1</sup> and Roy Maartens<sup>1</sup>

<sup>1</sup> *Institute of Cosmology and Gravitation, University of Portsmouth, Portsmouth PO1 2EG, UK*

<sup>2</sup> *Institut d'Astrophysique Spatiale, Université de Paris XI, bâtiment 120-121, Centre universitaire d'Orsay, 91400 Orsay CEDEX, France*

24 October 2018

## ABSTRACT

We consider a phenomenological model for a coupling between the dark matter and dark energy fluids and investigate the sensitivity of a weak lensing measurement for constraining the size of this coupling term. Physically, the functional form of the coupling term in our model describes the decay of dark matter into dark energy. We present forecasts for tomographic measurements of the weak shear bispectrum for the DUNE experiment in a Fisher-matrix formalism, where we describe the nonlinearities in structure formation by hyper-extended perturbation theory. Physically, CDM decay tends to increase the growth rate of density perturbations due to higher values for the CDM density at early times, and amplifies the lensing signal because of stronger fluctuations in the gravitational potential. We focus on degeneracies between the dark energy equation of state properties and the CDM decay constant relevant for structure formation and weak lensing. A typical lower bound on the CDM decay time  $\approx 7.7/H_0 = 75.3 \text{ Gyr}/h$  which could be provided by DUNE would imply that it would not be possible to produce the dark energy content of the universe by CDM decay within the age of the Universe for a constant equation of state parameter of  $w$  close to  $-1$ .

**Key words:** cosmology: gravitational lensing, large-scale structure, methods: analytical

## 1 INTRODUCTION

Dark energy as a cosmological fluid is evoked for explaining the late-time cosmic acceleration, which has been observed in a number of channels, e.g. the cosmic microwave background (CMB) anisotropies (Spergel et al. 2003) and the integrated Sachs-Wolfe-effect (Boughn & Crittenden 2003; Nolta et al. 2003; Giannantonio et al. 2006, 2008; Rassat et al. 2007). The numerical similarity of the values of the dark energy density  $\Omega_\phi \approx 0.75$  and the matter density  $\Omega_m \approx 0.25$  constitutes the coincidence problem: Why is the ratio  $\Omega_\phi/\Omega_m = O(1)$  today, or, why is the Hubble expansion dominated by dark energy after the formation of galaxies and the large-scale structure?

We focus on coupled models of dark energy proposed by (see Valiviita 2008; Boehmer et al. 2008), where the dark energy (DE) is generated by decay of dark matter (CDM). The CDM decay rate  $\Gamma$  is a constant free parameter, in addition to the matter density  $\Omega_m$  and the equation of state  $w$  of the dark energy. The time evolution of the matter density  $\rho_m$  and the dark energy density  $\rho_\phi$  is described by the energy balance equations (Boehmer et al. 2008), which can be written in matrix form as

$$\partial_t \begin{pmatrix} \rho_m \\ \rho_\phi \end{pmatrix} + \begin{pmatrix} 3H + \Gamma & 0 \\ -\Gamma & 3H(1+w) \end{pmatrix} \begin{pmatrix} \rho_m \\ \rho_\phi \end{pmatrix} = 0, \quad (1)$$

with the Friedmann constraint  $H^2 = \frac{1}{3}(\rho_m + \rho_\phi)$ . Note that the baryons are not coupled to dark energy, since this would be subject to severe constraints from ‘fifth-force’ experiments. We will neglect the baryons (and the radiation) in our analysis, which should not be a serious limitation, however, due to the fact that the baryon fraction  $f_b = \Omega_b/\Omega_m \approx 0.16$  has a small numerical value.

We also assume a homogeneous dark energy fluid, even though the decay of CDM in structures will naturally lead to local overdensities of dark energy. If the dark energy sound speed has a value close to 1, the dark energy will diffuse rapidly away from the dark matter structures and constitute a homogeneous fluid. Furthermore, the density fluctuations measured by weak lensing are only mildly overdense such that this assumption may be justified. Furthermore, we will work with the Newtonian Poisson equation and not the full general relativistic expression (Olivares et al. 2006), which is justified as the dark energy is assumed to be homogeneous.

Boehmer et al. (2008) provide a thorough discussion of the background dynamics of such a cosmology in the case where the dark energy is an exponential quintessence field. In order to analyse the growth of structure and weak lensing, we will use a simplified, phenomenological model of dark energy by introducing a parametrised time-variable equation of state. We aim to model a tomographic weak lensing measurement, and thus provide forecasts for parameter constraints and to quantify parameter degeneracies as one can expect from a deep weak lensing survey.

Gravitational lensing, in particular, has been shown to be

\* e-mail: bjoern.malte.schaefer@ias.u-psud.fr

a very powerful observational probe for investigating the influence of dark energy on structure formation and the geometry of the universe (Schneider et al. 1992; Mellier 1999; Bartelmann & Schneider 2001; Refregier 2003), even in the nonlinear regime of structure formation (Jain & Seljak 1997; Bernardeau et al. 1997; Benabed & Bernardeau 2001). Lensing data is best used in tomographic measurements for constraining dark energy equation of state properties (Hu 1999, 2002; Heavens 2003; Jain & Taylor 2003), where one either measures the power spectrum or the bispectrum of a weak lensing quantity (Kilbinger & Schneider 2005; Schneider & Bartelmann 1997; Bernstein & Jain 2004; Dodelson & Zhang 2005). Supplementing the recent paper by La Vacca & Colombo (2008), who derived lensing bounds on interacting models from weak lensing power spectra, we focus on bispectrum tomography, and we use a more general, albeit phenomenological cosmological model. Bispectra have the advantage that the perturbative treatment is easier to carry out and that they are sensitive on the transition from linear to nonlinear dynamics in structure formation.

After introducing the cosmological model and the peculiarities of gravitational lensing in the decaying CDM models in Sect. 2, we compute the weak lensing bispectrum and tomographic measurements in Sect. 3. Fisher-constraints on cosmological parameters are derived in Sect. 4 and the main results are summarised in Sect. 5. The parameter accuracies are forecast for the weak lensing survey proposed for the Dark UNiverse Explorer<sup>1</sup> (DUNE). For the fiducial model, we take a spatially flat  $\Lambda$ CDM cosmology with  $w = -1$ , adiabatic initial conditions and stable CDM ( $\Gamma = 0$ ). Specific parameter choices are  $H_0 = 100h$  km/s/Mpc with  $h = 0.72$ ,  $\Omega_m = 0.25$ ,  $\sigma_8 = 0.8$  and  $n_s = 1$ .

## 2 GROWTH FUNCTION AND WEAK LENSING

### 2.1 Decaying dark matter

The decay constant  $\Gamma$  will be expressed in units of the Hubble constant  $H_0$ . We rewrite eqn. (1) with the scale factor  $a$  as independent variable, and introduce the common parameterisation (Turner & White 1997; Chevallier & Polarski 2001; Linder & Jenkins 2003),

$$w(a) = w_0 + (1 - a)w_a. \quad (2)$$

The Hubble function  $H(a)$  is given by solving the differential equation with solutions for  $\rho_m(a)$  and  $\rho_\phi(a)$ ,

$$\frac{dH^2}{da} = -(\rho_m(a) + \rho_\phi(a) [1 + w(a)]). \quad (3)$$

The initial conditions are set at the present epoch  $a_0 = 1$ , and we integrate backwards to  $a = 10^{-2}$ . With the solution of  $H(a)$ , the comoving distance is

$$\chi(a) = \int_a^1 \frac{da}{a^2 H(a)}, \quad (4)$$

and the density parameters can be defined by normalising  $\Omega_m(a) = \rho_m(a)/\rho_{\text{crit}}(a)$  and  $\Omega_\phi(a) = \rho_\phi(a)/\rho_{\text{crit}}(a)$  with the critical density  $\rho_{\text{crit}} = 3H^2(a)/(8\pi G)$ . Table 1 gives an overview of the dark energy models considered in this paper.

The Hubble function and its first derivative are depicted in Fig. 1, where the SCDM-scaling is divided out,

model	$\Omega_m$	$\sigma_8$	$n_s$	$w_0$	$w_a$	$\Gamma$	CDM
$\Lambda$ CDM	0.25	0.8	1	-1	0	0	stable
$\Lambda_\Gamma$ CDM	0.25	0.8	1	-1	0	$\frac{1}{3}$	decaying
$\phi$ CDM	0.25	0.8	1	$-\frac{1}{3}$	$-\frac{1}{3}$	0	stable
$\phi_\Gamma$ CDM	0.25	0.8	1	$-\frac{1}{3}$	$-\frac{1}{3}$	$\frac{1}{3}$	decaying

**Table 1.** Summary of the four primary dark energy models considered in this paper, where  $\Gamma$  is the CDM decay constant.

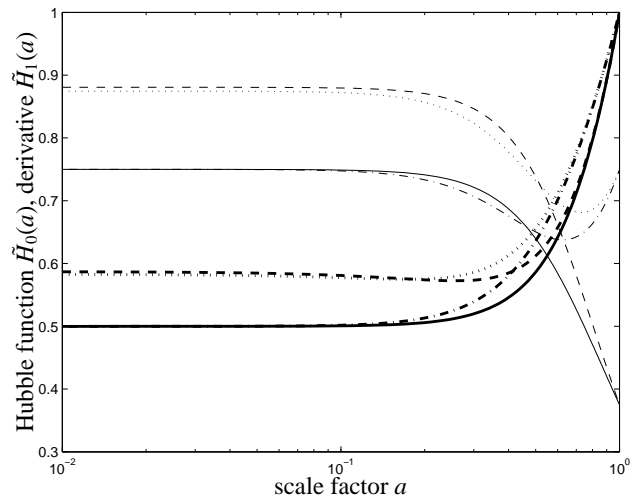


**Figure 1.** The scaled Hubble function  $\tilde{H}_0(a) = a^{3/2}H(a)/H_0$  (thick lines) and the derivative  $\tilde{H}_1(a) = a^{5/2}dH(a)/da/H_0$  (thin lines) in models with decaying CDM, in comparison to models with stable dark matter:  $\Lambda$ CDM (solid line),  $\Lambda_\Gamma$ CDM with  $\Gamma = \frac{1}{3}$  (dashed line),  $\phi$ CDM (dash-dotted line), and  $\phi_\Gamma$ CDM with  $\Gamma = \frac{1}{3}$  (dotted line).

$$\tilde{H}_n = a^{(2n+3)/2} \frac{d^n H(a)}{da^n H_0}. \quad (5)$$

An interesting feature, which will impact on the solution of the growth equation and on the Poisson equation, is the faster scaling of the Hubble function with the scale factor  $a$  in models with decay. This arises because the CDM density decreases not only by redshifting, which would be  $\propto a^{-3}$ , but also by decay. In addition, CDM decay causes the Hubble function to vary more gradually, which similarly can be achieved by introducing a variable equation of state of the dark energy fluid. Looking at the scaled first derivative of the Hubble function  $\tilde{H}_1(a)$  illustrates that the interplay between CDM decay and a variable dark energy equation of state gives rise to qualitatively new features in the Hubble function at scale factors  $0.2 \leq a \leq 0.5$ , compared to dark energy models with stable CDM.

### 2.2 Structure formation

The linear growth function  $D_+(a)$ , describing the homogeneous growth of structure,  $\delta(\mathbf{x}, a) = D_+(a)\delta(\mathbf{x}, 1)$  under Newtonian gravity, is obtained by solving the differential equation (Wang & Steinhardt 1998; Linder & Jenkins 2003),

$$\frac{d^2}{da^2} D_+(a) + \frac{1}{a} \left( 3 + \frac{d \ln H}{d \ln a} \right) \frac{d}{da} D_+(a) = \frac{3}{2a^2} \Omega_m(a) D_+(a), \quad (6)$$

which is still valid in decaying CDM models, as the decay does not affect the overdensity field  $\delta(\mathbf{x}) = (\rho(\mathbf{x}) - \langle \rho \rangle) / \langle \rho \rangle$ ,  $\langle \rho \rangle = \Omega_m \rho_{\text{crit}}$ .

<sup>1</sup> <http://www.dune-mission.net/>

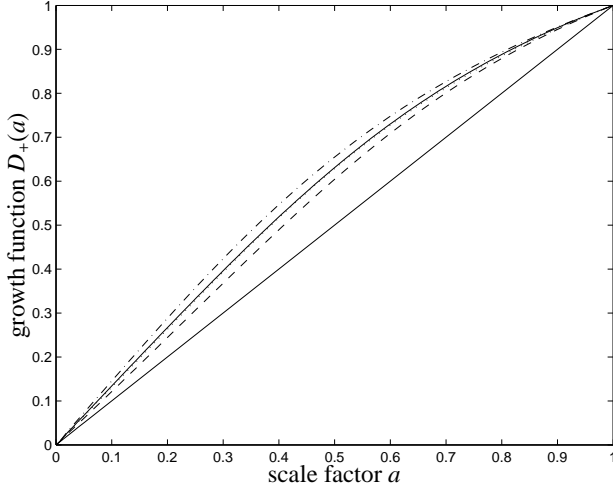


**Figure 2.** Growth function  $D_+(a)$  for four dark energy models:  $\Lambda$ CDM (solid line),  $\Lambda_\Gamma$ CDM with  $\Gamma = \frac{1}{3}$  (dashed line),  $\phi$ CDM (dash-dotted line), and  $\phi_\Gamma$ CDM with  $\Gamma = \frac{1}{3}$  (dotted line). Additionally, the growth function  $D_+(a) = a$  for SCDM is plotted (solid straight line).

The initial conditions for decaying CDM models are different compared to those of standard dark energy models, as the scaling of the Hubble function as well as the time-evolution of  $\Omega_m$  are changed by the decay. The asymptotic behaviour of the growth equation can be separated out by assuming  $D_+(a) \propto a^\alpha$  with a positive constant  $\alpha$  at early times. Substitution into eqn. (6) yields a quadratic equation for  $\alpha$ , which can be solved for an expression of  $\alpha$  depending on  $3 + d \ln H / d \ln a$  and  $\Omega_m(a)$ , evaluated at the initial time  $a_i$ . From that, one obtains the initial conditions  $D_+(a_i) = a_i^\alpha$  and  $dD_+/da = \alpha a_i^{\alpha-1}$ .

Fig. 2 shows the growth functions  $D_+(a)$  (normalised to unity today) in the four cosmologies considered. Evolving dark energy has the property of suppressing structure formation at an earlier time, which can be partially compensated by CDM decay (because the gravitational fields generated by the overdensity  $\delta(\mathbf{x})$  are stronger if  $\Omega_m(a)$  has a higher value), hinting at degeneracies between the equation of state parameters and the CDM decay rate. The  $\Lambda$ CDM and  $\phi_\Gamma$ CDM-models, for example, are almost indistinguishable. The influence of the two terms  $3 + d \ln H / d \ln a$  and  $\Omega_m(a)$  on the evolution of the growth factor  $D_+(a)$  is discussed in Appendix A.

### 2.3 Weak lensing

The non-standard scaling of the CDM density with scale factor makes it impossible to carry out a number of simplifications when deriving the weak lensing convergence. Substituting the critical density  $\rho_{\text{crit}}(a) = 3H^2(a)/(8\pi G)$  with  $\langle \rho \rangle(a) = \Omega_m(a)\rho_{\text{crit}}(a)$  into the expression  $\Delta\Phi = 4\pi G a^2 \langle \rho \rangle(a) \delta$  for the comoving Poisson equation yields

$$\Delta\Phi = \frac{3}{2} a^2 H^2(a) \Omega_m(a) \delta, \quad (7)$$

with explicit functions  $H(a)$  and  $\Omega_m(a)$ . Using this expression one obtains for the weak lensing convergence (Bartelmann & Schneider 2001)

$$\kappa(\chi) = \frac{3}{2c^2} \int_0^\chi d\chi' a^2 H^2(a) \Omega_m(a) \frac{\chi\chi' - \chi'^2}{\chi} \delta. \quad (8)$$

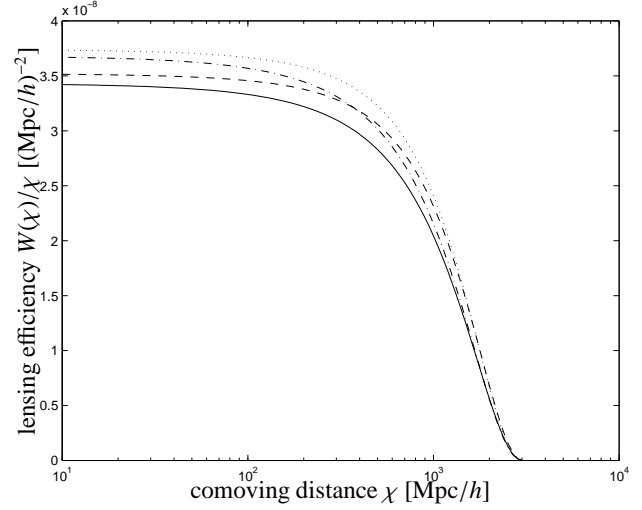


**Figure 3.** Lensing efficiency functions  $W(\chi)/\chi$  for the four dark energy models:  $\Lambda$ CDM (solid line),  $\Lambda_\Gamma$ CDM with  $\Gamma = \frac{1}{3}$  (dashed line),  $\phi$ CDM (dash-dotted line), and  $\phi_\Gamma$ CDM with  $\Gamma = \frac{1}{3}$  (dotted line), without subdivision into tomography bins.

Inclusion of the redshift distribution of background galaxies and reformulating the integration yields:

$$\kappa(\chi) = \frac{3}{2c^2} \int_0^\chi d\chi' a^2 H^2(a) \Omega_m(a) G(\chi)\chi' \delta, \quad (9)$$

where we abbreviated

$$G(\chi) = \int_{\chi'}^{\chi} d\chi'' p(z) \frac{dz}{d\chi''} \frac{\chi'' - \chi'}{\chi''}, \quad (10)$$

with the redshift distribution  $p(z)dz$  of the lensing galaxies. From that one finds an analogous expression for the convergence spectrum (Limber 1954),

$$C_\kappa(\ell) = \frac{9}{4c^4} \int_0^{\chi_H} d\chi G(\chi)^2 [aH(a)]^4 \Omega_m^2(\chi) D_+^2(a) P(k = \ell/\chi), \quad (11)$$

which results from projection of the CDM spectrum  $P(k)$ . The standard results are recovered by setting

$$\frac{\Omega_m(a)}{\Omega_m} = \frac{H_0^2}{a^3 H^2(a)}, \quad (12)$$

which is valid only for stable CDM-models. The lensing efficiency function  $W(\chi)$  can be isolated from the above expressions, yielding

$$W(\chi) = \frac{3}{2c^2} a^2 H^2(a) \Omega_m(a) G(\chi) \chi. \quad (13)$$

Lensing efficiency functions  $W(\chi)/\chi$  for the four exemplary cosmologies are given in Fig. 3: At low redshifts, models with evolving dark energy attain higher values for  $W(\chi)$  compared to models with a cosmological constant, and at high redshifts, models with decaying CDM have higher values for  $W(\chi)$  compared to models with stable CDM, with an interesting crossing at a distance of  $\approx 100$  Mpc/h. This behaviour is caused by the evolution of  $H(a)$  as discussed in the previous section and indicates that it is possible to increase the redshift at which the lensing signal originates by increasing  $\Gamma$  and by choosing an equation of state model with mean  $w$  close to  $-1$ .

Fig. 4 illustrates the impact of CDM decay on linear convergence power spectra: Models with decaying CDM exhibit larger values for the power spectrum, which is due to the fact that in these

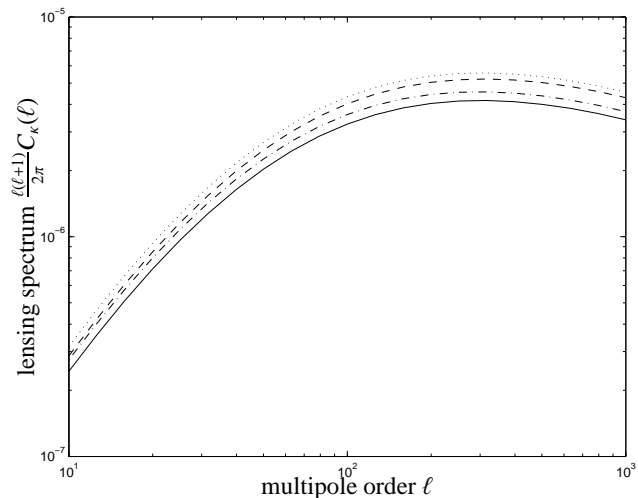


**Figure 4.** Linear convergence power spectra  $C_k(\ell)$  for the four specified dark energy models:  $\Lambda$ CDM (solid line),  $\Lambda_\Gamma$ CDM with  $\Gamma = \frac{1}{3}$  (dashed line),  $\phi$ CDM (dash-dotted line), and  $\phi_\Gamma$ CDM with  $\Gamma = \frac{1}{3}$  (dotted line), without subdivision into tomography bins.

models the matter density in the past was higher compared to models with stable CDM, which leads to stronger gravitational potentials and hence a stronger light deflection, which is described by the higher values of the lensing efficiency function  $W(\chi)$ , with a minor effect from the growth function  $D_+(a)$ . This feature might in fact be able to reconcile the high value for  $\sigma_8$  required by weak lensing surveys with the  $\sigma_8$  value following from CMB data, by generating high values for the lensing signal with a comparatively small value for  $\sigma_8$ , if one allows for CDM-decay.

In summary, the lensing signal measures a combination of structure growth  $D_+(a)$ , coupling strength  $\Omega_m(a)$  and geometrical factor  $\chi(a)$ , which all are influenced by the interaction term in the evolution equations for the dark matter and dark energy density and make up the form of the lensing efficiency  $W(\chi)$  and the finally the expression for the spectra  $C_k(\ell)$  and  $B_k(\ell_1, \ell_2, \ell_3)$ . The epoch-varying coupling of the light to the gravitational potential, due to the non-standard Poisson equation eqn. (7) is an important mechanism, which is not clearly treated in La Vacca & Colombo (2008). It is worth noting that models with interacting dark fluids constitute a new class of models in this respect, in comparison to models with non-interacting evolving dark energy.

Concerning the numerical evaluation, we generate a lookup table with 200 values of the relation between scale factor and comoving distance  $a(\chi)$ , the Hubble function  $H(a)$ , the growth function  $D_+(a)$ , the matter density parameter  $\Omega_m(a)$ , and finally the nonlinear wave vector  $k_{\text{nl}}$  for a given cosmological model and use cubic splines for interpolating between these values. Additionally, values for the tomography lensing efficiency functions  $G_i(\chi)$  for each redshift bin  $i$  are cached, as a function of comoving distance. These measures provide a significant speed-up in all computations, because we do not have to reevaluate the densities  $\rho_m$  and  $\rho_\phi$  for each time step, to solve for the Hubble function  $H(a)$  and the density parameter  $\Omega_m(a)$ , and use these results for computing the growth function  $D_+(a)$ , the comoving distance  $\chi$  and the lensing efficiency function  $G_i(\chi)$ .

### 3 WEAK LENSING BISPECTRUM TOMOGRAPHY

In this section we compile the necessary formulae for a tomographic measurement of the bispectrum and for a Fisher-matrix analysis in order to derive constraints on cosmological parameters including the CDM-decay rate  $\Gamma$  and to quantify parameter degeneracies, especially between  $\Gamma$  and the dark energy properties  $w_0$  and  $w_a$ , from a weak lensing observation.

We choose to consider a measurement of the bispectrum  $B_k(\ell_1, \ell_2, \ell_3)$  rather than a measurement of the spectrum  $C_k(\ell)$  because both yield very similar constraints on dark energy parameters, as shown by Takada & Jain (2003b, 2004), have a high covariance (which is difficult to quantify as it involves the computation of a 5-point correlation function) and are by no means independent measurements, and because of the fact that perturbation theory for describing the nonlinear evolution of the cosmic density field is in fact simpler for the 3-point functions compared to the 2-point functions: A consistent description of the nonlinear corrections to the 2-point function would involve contributions from both convergence fields perturbed to first order, and from one field perturbed to second order while the other field remains unperturbed. Contrarily, the leading contribution for the bispectrum involves the perturbation of a single field to first order, and decomposition of the resulting 4-point function with the Wick-theorem into a product of 2-point functions.

The most important difference between the spectra and bispectra concerning the line-of-sight integrations, however, is the fact that the spectrum is proportional to  $W^2(\chi)D_+^2(\chi)$ , whereas the bispectrum measures different powers of the lensing efficiency function and the growth rate, namely  $W^3(\chi)D_+^4(\chi)$ .

#### 3.1 Perturbation theory

For the linear power spectrum  $P(k)$ , which describes the fluctuation amplitude of the density field  $\delta(\mathbf{k})$ ,  $\langle \delta(\mathbf{k})\delta(\mathbf{k}') \rangle = (2\pi)^3 \delta_D(\mathbf{k} + \mathbf{k}')P(k)$ , we make the ansatz

$$P(k) \propto k^{n_s} T^2(k). \quad (14)$$

The shape of the transfer function  $T(k)$  is well approximated by the fitting formula suggested by Bardeen et al. (1986),

$$T(q) = \frac{\ln(1 + 2.34q)}{2.34q} \left( 1 + 3.89q + (16.1q)^2 + (5.46q)^3 + (6.71q)^4 \right)^{-\frac{1}{4}},$$

where the wave vector  $k = q\Gamma_s$  is rescaled with the shape parameter  $\Gamma_s$  (Sugiyama 1995),

$$\Gamma_s = \Omega_m h \exp \left( -\Omega_b \left( 1 + \frac{\sqrt{2}h}{\Omega_m} \right) \right). \quad (15)$$

The fluctuation amplitude is normalised to the value  $\sigma_8$  on the scale  $R = 8 \text{ Mpc}/h$ ,

$$\sigma_R^2 = \frac{1}{2\pi^2} \int dk k^2 W^2(kR) P(k), \quad (16)$$

with a Fourier-transformed spherical top-hat  $W(x) = 3j_1(x)/x$  as the filter function.  $j_\ell(x)$  denotes the spherical Bessel function of the first kind of order  $\ell$  (Abramowitz & Stegun 1972).

The first order contribution to the bispectrum  $B_\delta(\mathbf{k}_1, \mathbf{k}_2, \mathbf{k}_3)$  of the density field from nonlinear structure formation is given by (Fry 1984a,b; Takada & Jain 2003a):

$$B_\delta(\mathbf{k}_1, \mathbf{k}_2, \mathbf{k}_3) = \sum_{\substack{(i,j) \in \{1,2,3\} \\ i \neq j}} M(\mathbf{k}_i, \mathbf{k}_j) P_{\text{NL}}(k_i) P_{\text{NL}}(k_j), \quad (17)$$

with the classical mode coupling functions,

$$M(\mathbf{k}_i, \mathbf{k}_j) = \frac{10}{7} + \left( \frac{k_i}{k_j} + \frac{k_j}{k_i} \right) x + \frac{4}{7} x^2, \quad (18)$$

which is replaced by the mode coupling function in hyper-extended perturbation theory,

$$M(\mathbf{k}_i, \mathbf{k}_j) = \frac{10}{7} a(k_i) a(k_j) + b(k_i) b(k_j) \left( \frac{k_i}{k_j} + \frac{k_j}{k_i} \right) x + \frac{4}{7} c(k_i) c(k_j) x^2, \quad (19)$$

where  $x = \mathbf{k}_i \mathbf{k}_j / (k_i k_j)$  denotes the cosine of the angle between  $\mathbf{k}_i$  and  $\mathbf{k}_j$ . The coefficients  $a(k)$ ,  $b(k)$  and  $c(k)$  are given by (Scoccimarro & Frieman 1999; Scoccimarro & Couchman 2001):

$$a(k) = \frac{1 + \sigma_8^{-0.2}(z) \sqrt{0.7Q(n)} (q/4)^{n+3.5}}{1 + (q/4)^{n+3.5}}, \quad (20)$$

$$b(k) = \frac{1 + 0.4(n+3)q^{n+3}}{1 + q^{n+3.5}}, \quad (21)$$

$$c(k) = \frac{1 + \frac{4.5}{1.5+(n+3)^4} (2q)^{n+3}}{1 + (2q)^{n+3.5}}, \quad (22)$$

where the time evolution of the fluctuation amplitude is given by the linear growth function,  $\sigma_8(z) = D_+(z)\sigma_8$ . The wave vectors are rescaled with the nonlinear wave number,  $q \equiv k/k_{\text{NL}}$ . The logarithmic slope of the linear power spectrum,

$$n(k) = \frac{d \ln P(k)}{d \ln k} \quad (23)$$

can be straightforwardly determined with the polynomial fit to the transfer function  $T(k)$ . The nonlinear wave number at scale factor  $a$  is given by the scale at which the variance  $\sigma$  of the density fluctuations becomes unity,

$$\sigma^2 = \int_0^{k_{\text{NL}}} d^3 k D_+^2(z) P(k) = 1 \rightarrow 4\pi k_{\text{NL}}^3 D_+^2(z) P(k_{\text{NL}}) = 1. \quad (24)$$

Finally, the saturation parameter  $Q(n)$  can be computed from the logarithmic slope  $n$  of the linear CDM spectrum,

$$Q(n) = \frac{4 - 2^n}{1 + 2^{n+1}}. \quad (25)$$

Furthermore, we use the parameterisation proposed by Smith et al. (2003) for the nonlinear CDM spectrum  $P_{\text{NL}}(k)$  and its slow time evolution, which is particularly useful as the time evolution is parameterised with  $\Omega_m(a)$ .

### 3.2 Angular bispectra

The spherical bispectrum  $B_\kappa(\ell_1, \ell_2, \ell_3)$  is related to the flat-sky bispectrum  $B_\kappa(\ell_1, \ell_2, \ell_3)$  by (Miralda-Escude 1991; Kaiser 1992)

$$B_\kappa(\ell_1, \ell_2, \ell_3) \simeq \begin{pmatrix} \ell_1 & \ell_2 & \ell_3 \\ 0 & 0 & 0 \end{pmatrix} \sqrt{\frac{\prod_{p=1}^3 (2\ell_p + 1)}{4\pi}} B_\kappa(\ell_1, \ell_2, \ell_3), \quad (26)$$

where

$$\begin{pmatrix} \ell_1 & \ell_2 & \ell_3 \\ 0 & 0 & 0 \end{pmatrix}^2 = \frac{1}{2} \int_{-1}^{+1} dx P_{\ell_1}(x) P_{\ell_2}(x) P_{\ell_3}(x), \quad (27)$$

$x = \cos \theta$ , denotes the Wigner-3j symbol, which results from integrating over three Legendre polynomials  $P_\ell(x)$ . The Wigner-3j symbol cancels non-admissible configurations which would violate the triangle inequality  $|\ell_i - \ell_j| \leq \ell_k \leq \ell_i + \ell_j$  (Abramowitz & Stegun 1972). We use the Limber-equation (Limber 1954) in the flat-sky approximation,

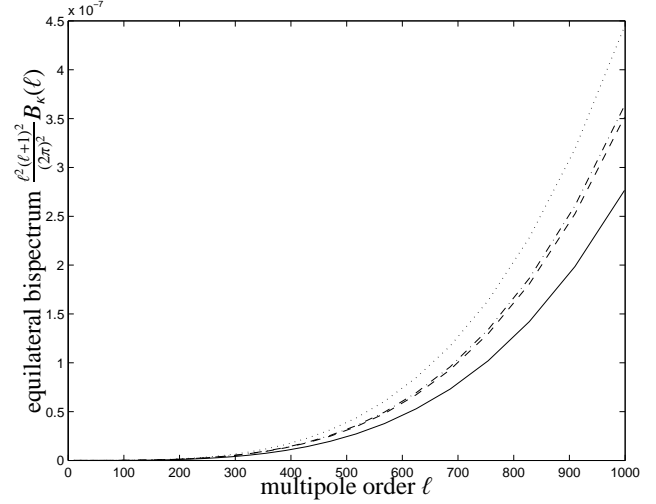


**Figure 5.** Equilateral convergence bispectra  $B_\kappa(\ell)$ :  $\Lambda$ CDM (solid line),  $\Lambda_\Gamma$ CDM with  $\Gamma = \frac{1}{3}$  (dashed line),  $\phi$ CDM (dash-dotted line), and  $\phi_\Gamma$ CDM with  $\Gamma = \frac{1}{3}$  (dotted line), for the entire galaxy sample.

$$B_\kappa(\ell_1, \ell_2, \ell_3) = \int_0^{x_H} d\chi \frac{1}{\chi^4} W^3(\chi) D_+^4(\chi) B_\kappa(\mathbf{k}_1, \mathbf{k}_2, \mathbf{k}_3), \quad (28)$$

with  $\mathbf{k}_p = \ell_p / \chi$ ,  $p = 1, 2, 3$ , for projection of the angular convergence bispectrum  $B_\kappa$ . The factorials in the Wigner-3j symbol are evaluated using the Stirling-approximation for the  $\Gamma$ -function,  $\Gamma(n+1) = n!$  with

$$\Gamma(x) \simeq \sqrt{2\pi} \exp(-x) x^{x-\frac{1}{2}} \quad (29)$$

for  $x \gg 1$  (Abramowitz & Stegun 1972). The resulting approximation for the Wigner-3j symbol overestimates the true value on average by  $\simeq 0.4\%$  in the relevant  $\ell$ -range. Weak lensing convergence bispectra resulting from this procedure are shown in Fig. 5 for the equilateral configuration. As in the case of the convergence spectra  $C_\kappa(\ell)$ , the bispectra  $B_\kappa(\ell_p)$  attain higher values in models with decaying CDM compared to those with stable CDM. This increase amounts to  $\simeq 10\%$ , and is observed independent of the equation of state of dark energy, where one observes a change of a few percent in the models with a cosmological constant relative to those with a varying equation of state.

Lensing convergence bispectra for isosceles triangles are given in Fig. 6, for  $\ell = 10^3$ . The plot suggests that the increase in power observed in decaying CDM models is present for all configurations, if the background galaxy distribution has a high average redshift, which is in fact expected for a change of cosmology on the homogeneous level. Again, typical differences between models with stable CDM and those with  $\Gamma = 1/3$  amount to  $\simeq 10\%$ , irrespective of the opening angle of the triangle.

Fig. 7 illustrates the configuration dependence of the weak lensing bispectra, for  $\ell_3 = 1000$ . In particular, the plot shows the configuration dependence variable  $R_{\ell_3}(\ell_1, \ell_2)$ ,

$$R_{\ell_3}(\ell_1, \ell_2) = \frac{\ell_1 \ell_2}{\ell_3^2} \sqrt{\frac{B(\ell_1, \ell_2, \ell_3)}{B(\ell_3, \ell_3, \ell_3)}}, \quad (30)$$

for  $\ell_3 = 10^3$ . Differences in cosmology are cancelled in first order in this expression, and for that reason the plot only shows the bispectrum configuration dependence for the fiducial  $\Lambda$ CDM model.

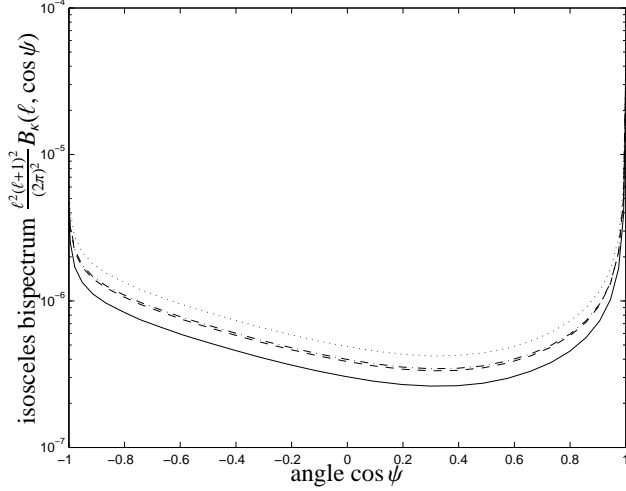


**Figure 6.** Isosceles convergence bispectra  $B_\kappa(\ell, \cos\psi)$ :  $\Lambda$ CDM (solid line),  $\Lambda_r$ CDM with  $\Gamma = \frac{1}{3}$  (dashed line),  $\phi$ CDM (dash-dotted line), and  $\phi_r$ CDM with  $\Gamma = \frac{1}{3}$  (dotted line), for the entire galaxy sample as a function of the cosine of the opening angle  $\psi$ . The angular scale is fixed to  $\ell_1 = \ell_2 = 10^3$ .

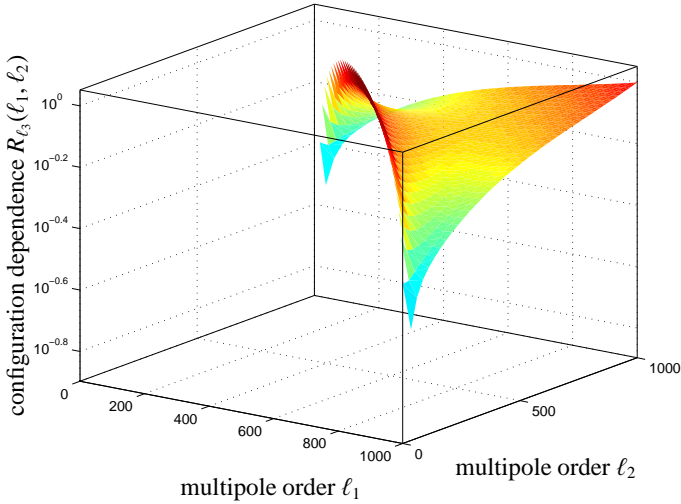


**Figure 7.** Convergence bispectrum configuration dependence  $R_{\ell_3}(\ell_1, \ell_2)$  for  $\ell_3 = 10^3$ , without subdivision into tomography bins. Non-admissible triangle configurations violating the inequality  $|\ell_i - \ell_j| \leq \ell_k \leq \ell_i + \ell_j$  would occupy the left empty side of the plot.

### 3.3 Bispectrum tomography

In the case of bispectrum tomography, where the background galaxies are divided in to two or more redshift bins ( $i, j, k$ ), eqn. (28) generalises to

$$B_{(ijk)}(\ell_1, \ell_2, \ell_3) = \int_0^{\chi_H} d\chi \frac{W_i(\chi)W_j(\chi)W_k(\chi)}{\chi^4} D_+^4(\chi) B_\delta(\mathbf{k}_1, \mathbf{k}_2, \mathbf{k}_3), \quad (31)$$

with individual weighting functions

$$W_i(\chi) = \begin{cases} \frac{3}{2c^2} a^2 H^2(a) \Omega_m(a) G_i(\chi) \chi, & \chi \leq \chi_{i+1} \\ 0, & \chi > \chi_{i+1}, \end{cases} \quad (32)$$

where the lensing-kernel weighted redshift distribution is given by

$$G_i(\chi) = \int_{\max(\chi, \chi_i)}^{\chi_{i+1}} d\chi' p(z) \frac{dz}{d\chi'} \frac{\chi' - \chi}{\chi'}. \quad (33)$$

$n$	$\Delta\Omega$	$f_{\text{sky}}$	$z_0$	$\sigma_\epsilon$
$4.7 \times 10^8$	$2\pi$	$\frac{1}{2}$	0.64	0.3

**Table 2.** Characteristics of the weak lensing survey of the Dark UNiverse Explorer (DUNE), in terms of galaxy number  $n$  per sterad (corresponding to a galaxy density of 40/arcmin<sup>2</sup>), solid angle  $\Delta\Omega$ , sky fraction  $f_{\text{sky}}$ , survey depth  $z_0$  and intrinsic ellipticity dispersion  $\sigma_\epsilon$  of the galaxy sample.

The tomography bins are chosen to contain equal numbers of background galaxies, which are distributed in redshift  $z$  according to (Smail et al. 1995),

$$p(z)dz = p_0 \left(\frac{z}{z_0}\right)^2 \exp\left(-\left(\frac{z}{z_0}\right)^\beta\right) dz \quad \text{with} \quad \frac{1}{p_0} = \frac{z_0}{\beta} \Gamma\left(\frac{3}{\beta}\right), \quad (34)$$

where the distribution is characterised by the parameters  $\beta = \frac{3}{2}$  and  $z_0 = 0.64$  (corresponding to a median redshift of  $z_{\text{med}} = 0.9$ , c.f. Appendix B). We will consider 2-bin tomography, because any finer subdivision does not necessarily improve the bounds on cosmological parameters due to the high covariance of the signal originating from different tomography bins, as discussed in Takada & Jain (2003b, 2004).

## 4 PARAMETER CONSTRAINTS

We use a Fisher-matrix approach (Tegmark et al. 1997) for estimating the accuracy of the determination the cosmological parameters  $\Omega_m, \sigma_8$ , the dark energy properties  $w_0, w_a$  and the CDM decay rate  $\Gamma$  for the weak lensing survey to be carried out by the DUNE experiment. The most important characteristics of DUNE are summarised in Table 2.

### 4.1 Bispectrum covariances

The observed bispectra  $\tilde{B}_{(ijk)}(\ell_1, \ell_2, \ell_3)$  are unbiased estimates of the true bispectra  $B_{(ijk)}(\ell_1, \ell_2, \ell_3)$ ,

$$\tilde{B}_{(ijk)}(\ell_1, \ell_2, \ell_3) \simeq B_{(ijk)}(\ell_1, \ell_2, \ell_3), \quad (35)$$

because the intrinsic ellipticity distribution  $p(\epsilon)d\epsilon$  of the background galaxies is assumed to be skewless. But  $p(\epsilon)d\epsilon$  has a finite width  $\sigma_\epsilon$ , which impacts on the observed power spectra  $\tilde{C}_{ij}(\ell)$  (Kaiser 1998; Hu 1999),

$$\tilde{C}_{(ij)}(\ell) = C_{(ij)}(\ell) + \delta_{ij} \frac{\sigma_\epsilon^2}{n_i}. \quad (36)$$

$n_i$  is the number of galaxies per steradian in the tomography bin  $i$ ,

$$n_i = n \int_{\chi_i}^{\chi_{i+1}} d\chi' p(z) \frac{dz}{d\chi'}, \quad (37)$$

with the total number of galaxies per steradian  $n$ . The bispectrum covariance for tomography, which is diagonal in  $\ell_p$ ,  $p = 1, 2, 3$ , is approximated by (Hu 2000; Takada & Jain 2003b, 2004)

$$\text{Cov} [B_{(ijk)}(\ell_p) B_{(lmn)}(\ell_p)] = \frac{\Delta(\ell_1, \ell_2, \ell_3)}{f_{\text{sky}}} \tilde{C}_{(ii)}(\ell_1) \tilde{C}_{(jm)}(\ell_2) \tilde{C}_{(kn)}(\ell_3), \quad (38)$$

where the function  $\Delta(\ell_p)$  counts the multiplicity of triangle configurations and is defined as

$$\Delta(\ell_1, \ell_2, \ell_3) = \begin{cases} 6, & \ell_1 = \ell_2 = \ell_3 \\ 2, & \ell_i = \ell_j \text{ for } i \neq j \\ 1, & \ell_1 \neq \ell_2 \neq \ell_3 \neq \ell_1. \end{cases} \quad (39)$$

$f_{\text{sky}}$  denotes the fraction of the observed sky. It is worth noting that the bispectra  $B_{(ijk)}(\ell_1, \ell_2, \ell_3)$  are invariant under permutations of the bin indices. Because of that, there are 4 independent bispectra for 2-bin tomography, which can be conveniently indexed with the number  $q = 2^i + 2^j + 2^k$ .

## 4.2 Fisher matrices

The Fisher matrix  $F_{\mu\nu}^{\text{GL}}$  for the parameter space consisting of  $x \in \{\Omega_m, \sigma_8, w_0, w_a, \Gamma, h\}$  is constructed with  $\Lambda$ CDM as the fiducial cosmological model. Particularly, for measurements of the weak lensing bispectrum  $B_{(ijk)}(\ell_1, \ell_2, \ell_3)$ , one obtains:

$$F_{\mu\nu}^{\text{GL}} = \sum_{\ell_p=\ell_{\min}}^{\ell_{\max}} \sum_{\substack{(i,j,k) \\ (l,m,n)}} \frac{\partial B_{(ijk)}(\ell_p)}{\partial x_\mu} (\text{Cov}[B_{(ijk)}B_{(lmn)}])^{-1} \frac{\partial B_{(lmn)}(\ell_p)}{\partial x_\nu}, \quad (40)$$

with  $\ell_p \in \{\ell_1, \ell_2, \ell_3\}$ . The summation is carried out with the condition  $\ell_1 \leq \ell_2 \leq \ell_3$ , such that every triangle configuration is counted once, between the limits  $\ell_{\min} = 10^2$  and  $\ell_{\max} = 2 \times 10^3$ . The indices  $i, j, k$  and  $l, m, n$  run over the tomography bins.

Following Takada & Jain (2003b, 2004), we use binned summations in the multipoles  $\ell_1$  and  $\ell_2$ , but carry out an unbinned summation in  $\ell_3$  in order to account for the vanishing Wigner-3j symbol if  $\sum_p \ell_p$  is an odd number and for the sign change of the Wigner-3j symbol depending on whether  $\sum_p \ell_p \bmod 4$  vanishes or not. Using  $\Delta\ell_1 = \Delta\ell_2 = 25$ , the computational load is reduced by three orders of magnitude, as we have to compute  $2 \times 10^7$  triangles instead of  $3 \times 10^{10}$  triangles, for  $l_{\max} = 2 \times 10^3$ . Using binned summation in two variables is well justified, given the smooth variation of the bispectrum illustrated in Fig. 7. The scale on which the numerical derivatives are computed corresponds to a 5% variation for  $\Omega_m, \sigma_8$  and  $h$  and to a 10% variation for the dark energy parameters  $w_0, w_a$  and  $\Gamma$ .

We would like to emphasise at this point that our Fisher-analysis implicitly assumes priors on (i) spatial flatness,  $\Omega_m + \Omega_\phi = 1$ , which affects all geometrical measures, (ii) the baryon density  $\Omega_b$ , which adds a correction to the shape parameter, and finally (iii) the slope  $n_s$  of the CDM spectrum  $P(k)$  for small wave numbers  $k$ . We neglect the influence of  $\Omega_b$ , because the baryons cause only a minor correction to the shape parameter, and keep  $n_s = 1$  and  $\Omega_m + \Omega_\phi = 1$  fixed, as they are both generic predictions of inflation and well tested by CMB observations. The parameter space considered here is motivated by the fact that  $\Omega_m, w_0, w_a$  and  $\Gamma$  all increase the lensing signal, either by their influence on the growth equation or by appearing in the Poisson equation, and are naturally degenerate with  $\sigma_8$ . As additional priors to the lensing measurement, we assume  $1\sigma$ -errors from PLANCK CMB observations with the numerical values  $\Delta h = 0.13$  and  $\Delta\sigma_8 = 0.01$  (Eisenstein et al. 1999). The priors are assumed to be diagonal,  $F_{\mu\nu}^{\text{CMB}} = \delta_{\mu\nu}/\sigma_\mu^2$ , and added to the lensing Fisher matrix  $F_{\mu\nu}^{\text{GL}}$ ,

$$F_{\mu\nu} = F_{\mu\nu}^{\text{GL}} + F_{\mu\nu}^{\text{CMB}}, \quad (41)$$

because the likelihoods of independent measurements can be multiplied and their  $\chi^2$ -functions added.

The diagonal elements of the inverse Fisher matrix give the Cramér-Rao bound on individual parameters,

$$\sigma_\mu = \sqrt{(F^{-1})_{\mu\mu}}, \quad (42)$$

which are compiled in Table 3 for 2-bin weak lensing tomography, with the enhancement of the measurement by including CMB-priors on  $\sigma_8$  and on  $h$ . Quite generally, weak lensing bispectrum

tomography		tomography+CMB
$\Omega_m = 0.25$	$\Delta\Omega_m = 0.029$	$\Delta\Omega_m = 0.011$
$\sigma_8 = 0.8$	$\Delta\sigma_8 = 0.023$	$\Delta\sigma_8 = 0.008$
$w_0 = -1$	$\Delta w_0 = 0.443$	$\Delta w_0 = 0.167$
$w_a = 0$	$\Delta w_a = 1.956$	$\Delta w_a = 0.542$
$\Gamma = 0$	$\Delta\Gamma = 0.187$	$\Delta\Gamma = 0.130$
$h = 0.72$	$\Delta h = 0.085$	$\Delta h = 0.033$

**Table 3.** Expected accuracy on the cosmological parameters from 2-bin weak lensing tomography, with  $\Lambda$ CDM as the fiducial cosmology. The second column adds a CMB prior on  $\sigma_8$  and  $h$  to the Fisher-matrix.

tomography with DUNE in conjunction with CMB priors provides percent errors on  $\Omega_m, \sigma_8$  and  $h$ , errors of the order of 20% on  $w_0$  and  $\Gamma$ , but a weak constraint on  $w_a$ , which is due to the fact that in comparing to the analysis by Takada & Jain (2004), the DUNE galaxy sample has a much lower median redshift (0.9 compared to 1.5) and hence a weaker lever arm on  $w_a$ .

The constraint on  $\Delta\Gamma \approx 0.13$  translates to a lower bound on the CDM lifetime of more than 7.7 Hubble times, corresponding to  $t_\Gamma \gtrsim 75.3/h$  Gyr. Limits on the CDM particle lifetime from lensing measurements of that order of magnitude may serve to exclude certain particle candidates, but we should emphasise that we investigate only a single decay channel with an unknown branching ratio  $b$ : If CDM has two decay modes with the probabilities  $b$  for decaying into dark energy and  $1-b$  for decaying into other products, with corresponding decay rates  $\Gamma_\phi$  (constrained by lensing) and  $\Gamma_\chi$ , the total decay rate is given by  $\Gamma = b\Gamma_\phi + (1-b)\Gamma_\chi$ .

The  $\chi^2$ -value for pairs of parameters  $(x_\mu, x_\nu)$  can be computed from the inverse  $(F^{-1})_{\mu\nu}$  of the Fisher matrix (Matsubara & Szalay 2002),

$$\chi^2 = \begin{pmatrix} \Delta x_\mu \\ \Delta x_\nu \end{pmatrix}^t \begin{pmatrix} (F^{-1})_{\mu\mu} & (F^{-1})_{\mu\nu} \\ (F^{-1})_{\nu\mu} & (F^{-1})_{\nu\nu} \end{pmatrix}^{-1} \begin{pmatrix} \Delta x_\mu \\ \Delta x_\nu \end{pmatrix}, \quad (43)$$

where  $\Delta x_\mu = x_\mu - x_\mu^{\Lambda\text{CDM}}$ . Specifically, the contour at

$$\Delta\chi_n^2 = -2 \ln \text{erfc}\left(\frac{n}{\sqrt{2}}\right), \quad (44)$$

encloses a fraction of  $\text{erf}(n/\sqrt{2})$  of parameter space, which corresponds to a confidence level of  $n\sigma$ .  $\text{erf}(x)$  and  $\text{erfc}(x) = 1 - \text{erf}(x)$  are the error function and the complementary error function, respectively (Abramowitz & Stegun 1972). The correlation coefficient  $r_{\mu\nu}$  is defined as

$$r_{\mu\nu} = \frac{(F^{-1})_{\mu\nu}}{\sqrt{(F^{-1})_{\mu\mu}(F^{-1})_{\nu\nu}}}, \quad (45)$$

and describes the degree of dependence between the parameters  $x_\mu$  and  $x_\nu$  by assuming numerical values close to 0 for independent, and close to 1 for strongly dependent parameters. Constraints on pairs  $(x_\mu, x_\nu)$  of cosmological parameters from the Fisher-analysis are compiled in Fig. 8, along with the respective correlation coefficient  $r_{\mu\nu}$ .

The CDM decay constant  $\Gamma$  is negatively correlated with  $\Omega_m$  because a simultaneous decrease of the matter density today as well as a increase in the decay constant leads to the same averaged matter density for the lensing signal. The degeneracies with  $w_0$  and  $w_a$  are such that  $w_0$  has to be de- and  $w_a$  increased in order to have the same lensing signal in models with non-vanishing  $\Gamma$ . The positive correlation of  $\Gamma$  with  $\sigma_8$  is a projection effect in the marginalisation driven by the tight constraints between  $\Omega_m, w_0$  and  $h$ , and the classi-

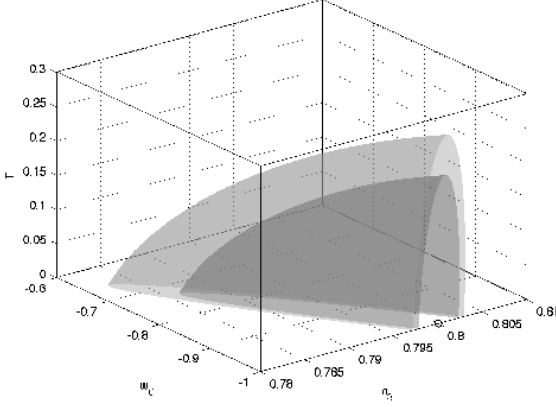


**Figure 9.** Fisher matrix constraints on the triplet  $(\sigma_8, w_0, \Gamma)$ , from weak lensing tomography including a CMB-prior on  $\sigma_8$  and  $h$ . The ellipsoids correspond to  $1\sigma$  and  $2\sigma$  intervals.

cal degeneracies between  $\Omega_m$  and  $\sigma_8$  (the power spectrum normalisation and the strength of the gravitational potentials) and between  $\Omega_m$  and  $h$  (the definition of the shape parameter) are recovered.

We would like to point out that the effective equation of state parameter  $w_{\text{eff}}$  may cross the boundary towards phantom models, for which  $w < -1$ ,

$$w_{\text{eff}} = w - \frac{\Gamma}{3h} \frac{\rho_m}{\rho_\phi} \xrightarrow{a=1} w_{\text{eff}} = w - \frac{\Gamma}{3} \frac{\Omega_m}{\Omega_\phi}, \quad (46)$$

with  $H(a) = H_0 h(a)$ , if decay is considered. Therefore, we mark the forbidden regions of parameter space in the relevant plots.

Generalising eqn. (43) to three parameters  $(x_\mu, x_\nu, x_\rho)$  yields

$$\chi^2 = \begin{pmatrix} \Delta x_\mu \\ \Delta x_\nu \\ \Delta x_\rho \end{pmatrix}^t \begin{pmatrix} (F^{-1})_{\mu\mu} & (F^{-1})_{\mu\nu} & (F^{-1})_{\mu\rho} \\ (F^{-1})_{\nu\mu} & (F^{-1})_{\nu\nu} & (F^{-1})_{\nu\rho} \\ (F^{-1})_{\rho\mu} & (F^{-1})_{\rho\nu} & (F^{-1})_{\rho\rho} \end{pmatrix}^{-1} \begin{pmatrix} \Delta x_\mu \\ \Delta x_\nu \\ \Delta x_\rho \end{pmatrix}. \quad (47)$$

In a 3-dimensional parameter space, the contours at  $\Delta\chi_1^2 \simeq 2.6124$  and  $\Delta\chi_2^2 \simeq 4.2222$  correspond to significance levels of  $1\sigma$  and  $2\sigma$ , respectively. Figs. 9 and 10 summarise simultaneous constraints on the triplets  $(\sigma_8, w_0, \Gamma)$  and  $(\Omega_m, \sigma_8, \Gamma)$ , respectively. The increase in lensing signal by either increasing  $\sigma_8$  or the dark energy equation of state  $w_0$  is illustrated in Fig. 9, with the weak degeneracy that models with decaying CDM require higher values of  $\sigma_8$ , for lensing at low redshift. Fig. 10, on the contrary, shows that  $\sigma_8$  can be decreased in models with decay if  $\Omega_m$  is increased at the same time.

## 5 SUMMARY

In this paper, we investigate the capability of the DUNE experiment to constrain the decay of dark matter into dark energy from the observation of the weak convergence bispectrum, in a tomographic measurement.

(i) Our cosmological model with CDM decaying into dark energy may provide an alternative explanation of the coincidence problem, i.e. the fact that the cosmic expansion is dominated by dark energy after structure formation. This is achieved by choosing a small value of the decay constant  $\Gamma$ . Decaying CDM naturally influences the Hubble function by providing dark energy, and by introducing a faster scaling of the matter density compared to  $\rho \propto a^{-3}$  in models with stable CDM.

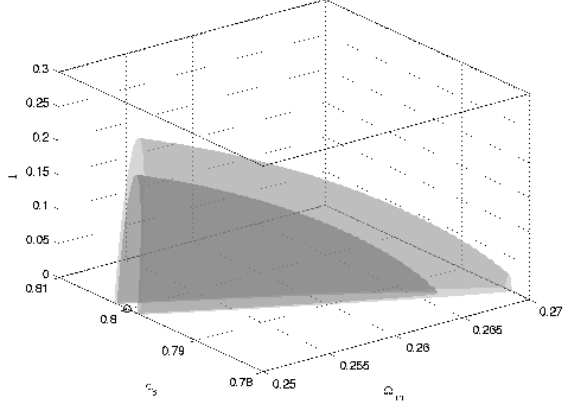


**Figure 10.** Fisher matrix constraints on the triplet  $(\Omega_m, \sigma_8, \Gamma)$ , from weak lensing tomography including a CMB-prior on  $\sigma_8$  and  $h$ . The ellipsoids correspond to  $1\sigma$  and  $2\sigma$  intervals.

(ii) We have neglected the contribution of baryons, whose density would just decrease  $\propto a^{-3}$ , because they are stable particles. This should not be a serious limitation, however, due to the fact that the baryon fraction  $f_b = \Omega_b/\Omega_m \simeq 0.16$  has a small numerical value. Models with decaying CDM have the interesting property, however, that the baryon fraction  $f_b = \rho_b/\rho_m$  is monotonically increasing with cosmic time.

(iii) The growth of structure is influenced in two ways: Firstly by the non-standard scaling of the density parameter  $\Omega_m$  which causes stronger gravitational potentials in the past in models with decaying CDM, and secondly by affecting the logarithmic derivative of the Hubble function, which is smaller in decaying models. These changes are naturally degenerate with models for dark energy with a varying equation of state. We work in the limit of the dark energy sound speed being close to  $c$ , such that dark energy can be considered homogeneous even though it originates by decay from clustered dark matter.

(iv) Similarly to the growth of structure, the coupling to of light to the matter in gravitational lensing is affected by the higher value of  $\Omega_m$ , which causes the gravitational potential  $\Phi$  induced by the overdensity field  $\delta$  to be stronger in decaying models. With this mechanism, models with decaying CDM can provide an explanation for the high values of  $\sigma_8$  required by cosmic shear experiments, and can be reconciled with measurements of  $\sigma_8$  from CMB observations.

(v) Weak lensing bispectrum tomography yields a relative accuracy on the determination of the dark energy equation of state parameters  $w_0, w_a$ , the CDM decay rate  $\Gamma$  of a tenth and percent accuracy on the parameters  $\Omega_m, \sigma_8$ , if CMB priors are included. The CDM decay rate  $\Gamma$  is naturally degenerate with the equation of state parameters  $w_0$  and  $w_a$ . The Fisher-analysis provides an upper bound on  $\Gamma$ , or equivalently, a lower bound on the CDM lifetime,  $t_\Gamma = 1/\Gamma > 7.7/H_0 \simeq 75.3 \text{ Gyr}/h$ . This limit might be useful to exclude certain CDM particle candidates, although we should emphasise here that we investigate a single decay channel only, and that the branching ratio of this particular channel would need to be known as well.

(vi) Comparing the lensing constraints on  $\Gamma$  to supernova constraints shows that differences in luminosity distance small: There is a 0.01% difference between  $\Lambda_\Gamma\text{CDM}$  and  $\Lambda\text{CDM}$  and a 1% difference between  $\Phi_\Gamma\text{CDM}$  and  $\Lambda\text{CDM}$  at  $z = 0.1$ . Moving to higher



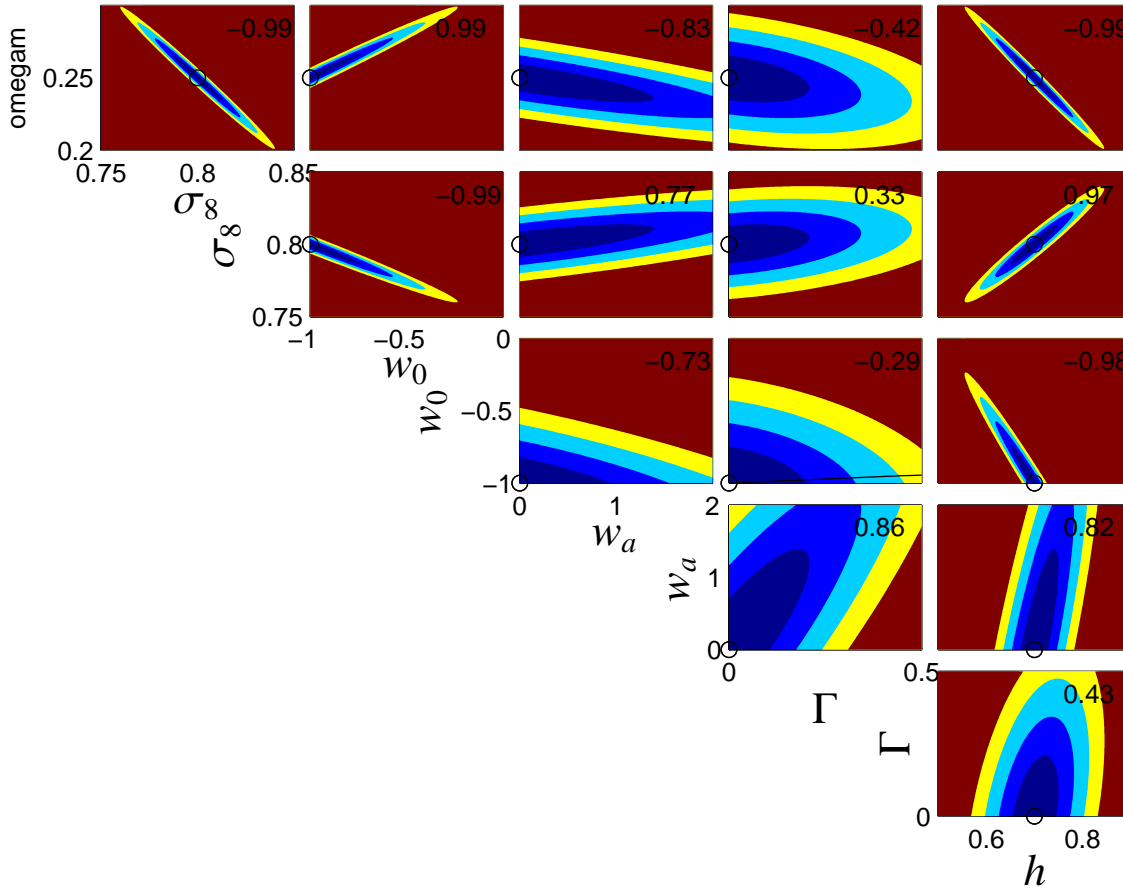


**Figure 8.** Constraints on cosmological parameters and the CDM decay rate from the Fisher-matrix analysis from weak lensing tomography. The choice for the fiducial cosmological model is  $\Omega_m = 0.25$ ,  $\sigma_8 = 0.8$ ,  $w_0 = -1$ ,  $w_a = 0$ ,  $\Gamma = 0$  and  $h = 0.72$  (marked by a circle). The ellipses correspond to  $1\sigma \dots 4\sigma$ . The correlation coefficient  $r_{\mu\nu}$  of the parameter pair  $(x_\mu, x_\nu)$  is given in the upper right corner of each panel (to two digits), and the excluded region of parameter space due to the phantom constraint eqn. (46) is below the line in the  $w_0$ - $\Gamma$  plot.

redshifts confirms the trend that the equation of state has a stronger influence on the luminosity distance than the CDM decay rate. At  $z = 1$ , one observes a 1% difference between  $\Lambda_\Gamma$ CDM and  $\Lambda$ CDM, but 7% difference between the stable dark energy models  $\Phi_\Gamma$ CDM and  $\Lambda$ CDM.

(vii) It is worth noting that models with decaying CDM are genuinely different from dark energy models concerning structure growth and observations which use gravitational interaction such as gravitational lensing. While it is always possible to construct an equation of state  $w(a)$  for a dark energy model with stable CDM that gives the identical Hubble function as a model with decaying CDM, the evolution of the density parameter  $\Omega_m(a)$  and the growth function  $D_+(a)$  breaks this degeneracy which would be different in the two cases. For that reason, the combination of probes of cosmic structure growth and the expansion history are able to distinguish between the two families of models, which would not be possible with e.g. supernova observations alone.

In addition, we plan to provide prospective constraints from the integrated Sachs-Wolfe effect, which is promising as it originates at higher redshifts, and directly measures the derivative  $d \ln \rho_m(a) / d \ln a$ , which is  $\neq -3$  in decaying CDM models. In summary we would like to stress that CDM-decay would be an elegant solution to the coincidence problem, and that its central parameter  $\Gamma$  is well measurable by future lensing surveys.

## ACKNOWLEDGEMENTS

We would like to thank David Bacon, Rob Crittenden, and Lukas Hollenstein for valuable comments, and Alexandre Refregier for providing the characteristics of the DUNE survey. BMS acknowledges support from an STFC postdoctoral fellowship. GACC is supported by the Programme Alban, the European Union Programme of High Level Scholarships for Latin America, scholarship No. E06D103604MX and the Mexican National Council for Science and Technology, CONACYT, scholarship No. 192680. The work of RM is supported by STFC.

## REFERENCES

- Abramowitz M., Stegun I. A., 1972, Handbook of Mathematical Functions. Handbook of Mathematical Functions, New York: Dover, 1972
- Bardeen J. M., Bond J. R., Kaiser N., Szalay A. S., 1986, ApJ, 304, 15
- Bartelmann M., Schneider P., 2001, Physics Reports, 340, 291
- Benabed K., Bernardeau F., 2001, Phys. Rev. D, 64, 083501
- Bernardeau F., van Waerbeke L., Mellier Y., 1997, A&A, 322, 1
- Bernstein G., Jain B., 2004, ApJ, 600, 17

Boehmer C. G., Caldera-Cabral G., Lazkoz R., Maartens R., 2008, ArXiv 0801.1565, 801

Boughn S. P., Crittenden R. G., 2003, in Holt S. H., Reynolds C. S., eds, The Emergence of Cosmic Structure Vol. 666 of American Institute of Physics Conference Series, The Absence of the Integrated Sachs-Wolfe Effect: Constraints on a Cosmological Constant. pp 67–70

Chevallier M., Polarski D., 2001, International Journal of Modern Physics D, 10, 213

Dodelson S., Zhang P., 2005, Phys. Rev. D, 72, 083001

Eisenstein D. J., Hu W., Tegmark M., 1999, ApJ, 518, 2

Fry J. N., 1984a, ApJL, 277, L5

Fry J. N., 1984b, ApJ, 279, 499

Giannantonio T., Crittenden R. G., Nichol R. C., Scranton R., Richards G. T., Myers A. D., Brunner R. J., Gray A. G., Connolly A. J., Schneider D. P., 2006, Phys. Rev. D, 74, 063520

Giannantonio T., Scranton R., Crittenden R. G., Nichol R. C., Boughn S. P., Myers A. D., Richards G. T., 2008, ArXiv 0801.4380, 801

Heavens A., 2003, MNRAS, 343, 1327

Hu W., 1999, ApJL, 522, L21

Hu W., 2000, Phys. Rev. D, 62, 043007

Hu W., 2002, Phys. Rev. D, 66, 083515

Jain B., Seljak U., 1997, ApJ, 484, 560

Jain B., Taylor A., 2003, Physical Review Letters, 91, 141302

Kaiser N., 1992, ApJ, 388, 272

Kaiser N., 1998, ApJ, 498, 26

Kilbinger M., Schneider P., 2005, A&A, 442, 69

La Vacca G., Colombo L. P. L., 2008, ArXiv e-prints, 803

Limber D. N., 1954, ApJ, 119, 655

Linder E. V., Jenkins A., 2003, MNRAS, 346, 573

Matsubara T., Szalay A. S., 2002, ApJ, 574, 1

Mellier Y., 1999, ARA&A, 37, 127

Miralda-Escude J., 1991, ApJ, 380, 1

Nolta M. R., Devlin M. J., Dorwart W. B., Miller A. D., Page L. A., Puchalla J., Torbet E., Tran H. T., 2003, ApJ, 598, 97

Olivares G., Atrio-Barandela F., Pavón D., 2006, Phys. Rev. D, 74, 043521

Rassat A., Land K., Lahav O., Abdalla F. B., 2007, MNRAS, 377, 1085

Refregier A., 2003, ARA&A, 41, 645

Schneider P., Bartelmann M., 1997, MNRAS, 286, 696

Schneider P., Ehlers J., Falco E. E., 1992, Gravitational Lenses. Springer-Verlag Berlin Heidelberg New York.

Scoccimarro R., Couchman H. M. P., 2001, MNRAS, 325, 1312

Scoccimarro R., Frieman J. A., 1999, ApJ, 520, 35

Smail I., Hogg D. W., Blandford R., Cohen J. G., Edge A. C., Djorgovski S. G., 1995, MNRAS, 277, 1

Smith R. E., Peacock J. A., Jenkins A., White S. D. M., Frenk C. S., Pearce F. R., Thomas P. A., Efstathiou G., Couchman H. M. P., 2003, MNRAS, 341, 1311

Spergel D. N., Verde L., Peiris H. V., Komatsu E., Nolta M. R., Bennett C. L., Halpern M., Hinshaw G., Jarosik N., Kogut A., Limon M., Meyer S. S., Page L., Tucker G. S., Weiland J. L., Wollack E., Wright E. L., 2003, ApJS, 148, 175

Sugiyama N., 1995, ApJS, 100, 281

Takada M., Jain B., 2003a, MNRAS, 340, 580

Takada M., Jain B., 2003b, MNRAS, 344, 857

Takada M., Jain B., 2004, MNRAS, 348, 897

Tegmark M., Taylor A. N., Heavens A. F., 1997, ApJ, 480, 22

Turner M. S., White M., 1997, Phys. Rev. D, 56, 4439

Valiviita J., 2008, Phys. Rev. D. in preparation

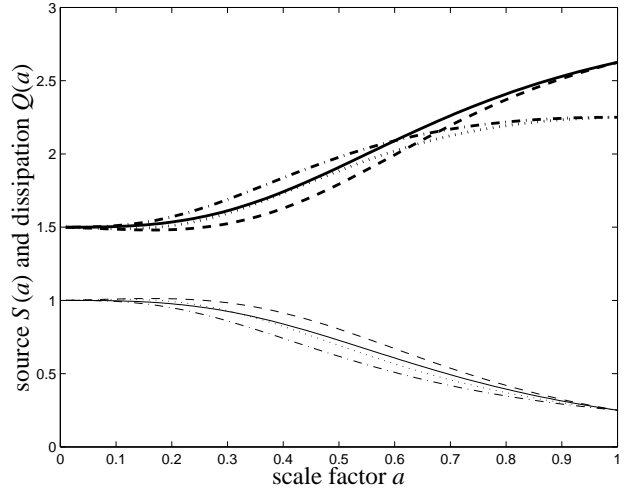


**Figure A1.** Comparison of the dissipation term  $Q(a) = 3 + d \ln H / d \ln a$  (thick lines) and the source term  $S(a) = \Omega_m(a)$  (thin lines) in the growth equation, for  $\Lambda$ CDM (solid line),  $\Lambda_\Gamma$ CDM with  $\Gamma = \frac{1}{3}$  (dashed line),  $\phi$ CDM (dash-dotted line), and  $\phi_\Gamma$ CDM with  $\Gamma = \frac{1}{3}$  (dotted line).

Wang L., Steinhardt P. J., 1998, ApJ, 508, 483

## APPENDIX A: GROWTH FUNCTION

The growth function  $D_+(a)$  is a solution to the differential equation

$$\frac{d^2}{da^2} D_+(a) + \frac{1}{a} \left( 3 + \frac{d \ln H}{d \ln a} \right) \frac{d}{da} D_+(a) = \frac{3}{2a^2} \Omega_m(a) D_+(a). \quad (\text{A1})$$

Fig. A1 compares the source term  $S(a) = \Omega_m(a)$  with the dissipation term  $Q(a) = 2 - q = 3 + d \ln H / d \ln a$  for the exemplary cosmologies. Dark energy with a variable equation of state increases the dissipation term and decreases the source term of the growth equation, and suppresses growth relative to  $\Lambda$ CDM. CDM decay is able to compensate this effect, by enhancing growth due to decreasing the dissipation term  $Q(a)$  even below the value of 1.5, and a slower increase at late times. At the same time, the matter density remains closer to the critical density for a longer period of time, until the CDM decay causes it to decrease to the current value.

The near-degeneracy of the growth functions  $D_+(a)$  in  $\Lambda$ CDM and  $\phi_\Gamma$ CDM are explained by the fact that they show very similar evolutions of  $\Omega_m(a)$ , and up to  $z = 1$ , the damping term  $Q(a)$  is almost identical between the two models. At smaller redshifts, the damping as well as the source term are both smaller compared to  $\Lambda$ CDM, with a compensating effect on the evolution of  $D_+(a)$ .

## APPENDIX B: REDSHIFT DISTRIBUTION

The unit-normalised redshift distribution  $p(z)dz$  (Smail et al. 1995),

$$p(z)dz = p_0 \left( \frac{z}{z_0} \right)^2 \exp \left( - \left( \frac{z}{z_0} \right)^\beta \right) dz \quad \text{with} \quad \frac{1}{p_0} = \frac{z_0}{\beta} \Gamma \left( \frac{3}{\beta} \right), \quad (\text{B1})$$

the cumulative distribution  $P(z)$ ,

$$P(z) = \int_0^z dz' p(z'), \quad (\text{B2})$$

and the redshift boundaries for 2-bin ( $z = 0.90$ ) and 3-bin ( $z = 0.72$  and 1.11) tomography are shown in Fig. B1. The parameters are

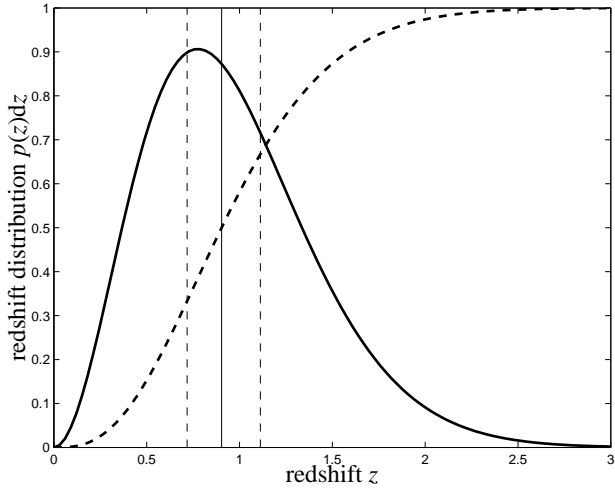


**Figure B1.** Differential distribution  $p(z)dz$  (thick solid line) and cumulative distribution  $P(z) = \int_0^z dz' p(z')$  (thick dashed line) of the lensed galaxies observed by DUNE, with redshift bins for 2-bin (thin solid line) and 3-bin (thin dashed line) weak lensing tomography.

$z_0 = 0.64$  (corresponding to a median redshift of  $z_{\text{med}} = 0.9$ ) and  $\beta = \frac{3}{2}$ . These bins are chosen in such a way that there are equal number of background galaxies in each tomography bin. This has the consequence that the noise contribution  $\sigma_\epsilon^2/n_i$  to the spectral measurements from each bin is equal. Although convenient, this choice of redshift binning is by no means optimised for providing the maximal accuracy in the measurement of cosmological parameters. It should be possible, however, to perform an iterative procedure with a coarse determination to begin with, and a subsequent choice of tomography bins which maximises the accuracy.

This paper has been typeset from a  $\text{\TeX}/\text{\LaTeX}$  file prepared by the author.